

Kantorovich–Rubinstein–Wasserstein distance between overlapping attractor and repeller

Cite as: Chaos 30, 073114 (2020); doi: 10.1063/5.0007230

Submitted: 11 March 2020 · Accepted: 16 June 2020 ·

Published Online: 7 July 2020



View Online



Export Citation



CrossMark

Vladimir Chigarev,¹  Alexey Kazakov,^{1,2,a)}  and Arkady Pikovsky^{1,3} 

AFFILIATIONS

¹National Research University Higher School of Economics, 25/12 Bolshaya Pecherskaya Ulitsa, 603155 Nizhny Novgorod, Russia

²Lobachevsky State University of Nizhny Novgorod, 23 Prospekt Gagarina, 603950 Nizhny Novgorod, Russia

³Institute of Physics and Astronomy, University of Potsdam, Karl-Liebknecht-Str. 24/25, 14476 Potsdam-Golm, Germany

^{a)}Author to whom correspondence should be addressed: kazakovdz@yandex.ru

ABSTRACT

We consider several examples of dynamical systems demonstrating overlapping attractor and repeller. These systems are constructed via introducing controllable dissipation to prototypic models with chaotic dynamics (Anosov cat map, Chirikov standard map, and incompressible three-dimensional flow of the ABC-type on a three-torus) and ergodic non-chaotic behavior (skew-shift map). We employ the Kantorovich–Rubinstein–Wasserstein distance to characterize the difference between the attractor and the repeller, in dependence on the dissipation level.

Published under license by AIP Publishing. <https://doi.org/10.1063/5.0007230>

In studies of chaos and complex dynamics in dynamical systems, one usually distinguishes cases where the phase volume is conserved (conservative dynamics) and those where it decreases in time (dissipative dynamics). Recently, a mixed dynamics attracted much attention, where attractors (limiting sets forward in time) and repellers (limiting sets at the dynamics backward in time) overlap but do not coincide. Here, we introduce a simple way to generate such an overlapping by adding dissipation to the conservative systems in a special controlled way. To characterize the difference between attractors and repellers, we suggest the use of the Kantorovich–Rubinstein–Wasserstein distance (KRWD). This concept, also called earth mover's distance, is a general tool defining minimal costs of “transportation” from one measure to another. In this work, we present the results of calculation of KRWDs for different examples of overlapping attractors and repellers.

I. INTRODUCTION

Studies of attractors and repellers are central in the nonlinear dynamics of dissipative dynamical systems. However, there are different notions and definitions of these objects, relevant in different situations. Mostly, often one deals with isolated attractors that

absorb, as time goes on, all the points from a whole neighborhood (see, e.g., Ref. 1). If the phase space of the system is closed (for example, a high-dimensional torus in the case of the phase dynamics or a sphere for a spin–torque oscillator) or a system is time-reversible,^{2,3} one can also consider the dynamics backward in time and define a repeller as an attractor of the backward dynamics. Isolated attractor and repeller do not overlap (but they can collide^{4–6}).

In Refs. 7 and 8, it has been demonstrated that the attractor and the repeller can overlap giving the so-called phenomenon of mixed dynamics (see Refs. 9–11 and references therein). In this case, it is convenient to speak not on topology of these sets, but on invariant measures. The invariant measures for the attractor and the repeller are different and both are fractal, but they can have the same support (in the examples below this will be the full phase space). For dissipative dynamics with a compact phase space, the phase volume decreases both by forward and backward iterations so that both the attractor and the repeller are fractal sets. They will evidently overlap if their supports are the full phase space (so that the box-counting dimensions are the dimension of the phase space). Higher-order dimensions are, however, smaller. It is worth noting that systems with such behavior can be ergodic and, even, hyperbolic.^{12,13} In this paper, we do not focus on the fractal properties of the attractor and the repeller but on the difference—distance—between them.

In our examples, we start with area-preserving two-dimensional maps which possess a uniform invariant measure by iterations both

forward and backward in time. Upon including dissipation (i.e., phase volume decreases in some regions and increases in other ones), the time-reversal symmetry is broken, and the attractor and the repeller invariant measures become different. We suggest to characterize the distance between these two measures with a well-established approach of the Kantorovich–Rubinstein–Wasserstein distance. This concept first appeared in the optimal transportation problem, where it is also known as the Earth Mover’s Distance (EMD). The idea is to find an optimal “transportation” of one measure to another with a proper definition of costs (which in most cases are just proportional to the ground distance multiplied with the transported mass). While this concept has been previously applied to characterize the difference between attractors of a dynamical system at different parameter values,^{14–16} to the best of our knowledge, it has not been suggested as a measure of the attractor–repeller difference. For other relations of the transportation problem to theory of dynamical systems, see Ref. 17.

The paper is organized as follows. In Sec. II, we introduce four basic models, three of them are maps given on a two-dimensional torus possessing the uniform invariant measure: the Anosov cat map, Chirikov standard map, and skew shift. We also define a convenient way to introduce dissipation to these systems, by employing a Möbius circle map,^{18,19} and illustrate appearing attractors and repellers. The fourth model is the incompressible three-dimensional flow of the ABC-type on a three-dimensional torus where dissipation is introduced straightforwardly. We present attractors and repellers in all these systems. In Sec. III, we define the Kantorovich–Rubinstein–Wasserstein distance and perform its numerical evaluation for the attractors and repellers. We discuss the results in Sec. IV. In the Appendix, we give some details on the computation of the KRW distance and evaluate computational complexity.

II. BASIC MODELS

In this section, we introduce four models to be explored numerically below. All these models have a compact phase space. First, we

will define three maps on a two-dimensional torus $0 \leq x, y < 1$. In these examples, quite a full understanding of attractors and repellers can be achieved. We will start with the “pure” cases where these maps conserve the phase-space volume (Jacobian is exactly 1), and then add dissipation. The fourth example is a smooth continuous-time dynamical system on a three-dimensional torus. Here, we can say less about the topological organization of the dynamics, rather we will rely on a numerical analysis of the Lyapunov exponents to show that indeed the attractor and the repeller exist in a certain range of parameters.

A. Three maps on the 2-torus

The first map is the Anosov cat map A,

$$\begin{aligned}x_{n+1} &= 2x_n + y_n \pmod{1}, \\y_{n+1} &= x_n + y_n \pmod{1}.\end{aligned}\quad (1)$$

This is a prominent example of conservative hyperbolic chaos,²⁰ see Fig. 1(a), demonstrating that the stable and the unstable manifolds of the saddle fixed point $O(0, 0)$ intersect transversally.

The second map is the Chirikov standard map C

$$\begin{aligned}x_{n+1} &= x_n + K \sin(2\pi y_n) \pmod{1}, \\y_{n+1} &= y_n + x_{n+1} \pmod{1}.\end{aligned}\quad (2)$$

This map is the prototypic example of Hamiltonian dynamics with a divided phase space.²¹ For small values of parameter K , the dynamics is nearly integrable, while for $K \gg 1$, it is predominantly chaotic. Chaos here is not hyperbolic because the stable and unstable manifolds of saddle points can possess tangencies [see Fig. 1(b)]. Thus, generally, elliptic (stable) periodic orbits are not excluded.²² Practically, one hardly observes regular islands for large enough values of K . Below, we adopt $K = 14/(2\pi)$.

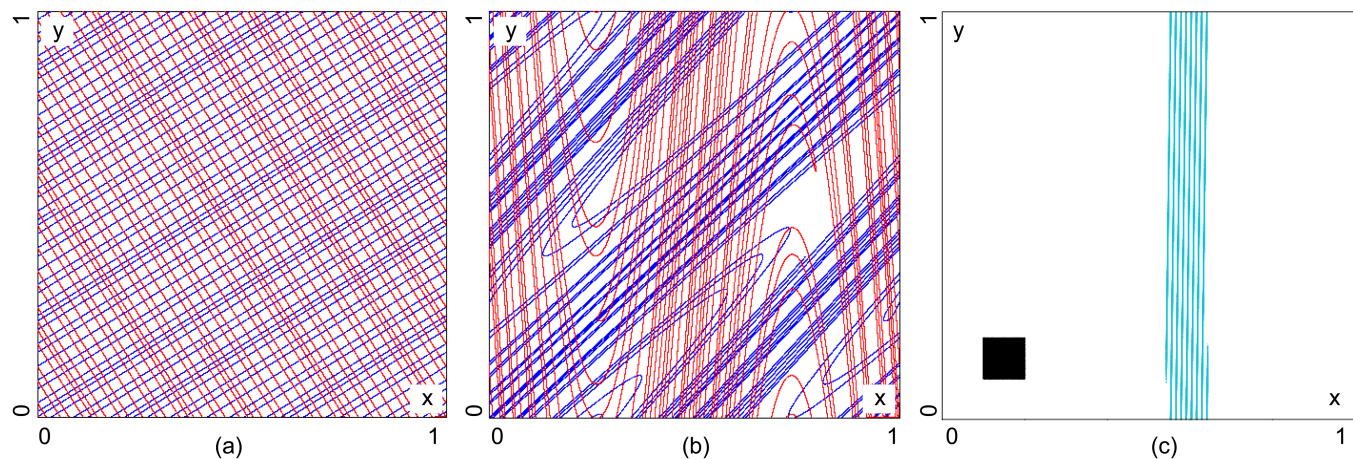


FIG. 1. Stable (in red) and unstable (in blue) invariant manifolds of $(0, 0)$ saddle fixed point for the Anosov cat map (1) [panel (a)] and the standard map (2) with $K = 14/(2\pi)$ [panel (b)]. Panel (c): the 80th image of the square $([0.1, 0.2] \times [0.1, 0.2])$ densely filled by initial conditions for the skew-shift map (3).

The third map is a linear skew shift over a circle rotation S ,

$$\begin{aligned} x_{n+1} &= x_n + y_n \pmod{1}, \\ y_{n+1} &= y_n + \omega \pmod{1}. \end{aligned} \tag{3}$$

This map is not chaotic, it has two zero Lyapunov exponents. It is known that for irrational ω , it is ergodic map on the torus.²³ Below, we fix this parameter as the inverse value to golden mean ($\omega = (\sqrt{5} - 1)/2$). In order to illustrate its ergodicity, we plot in Fig. 1(c) the n th iteration of a small rectangle $([0.1, 0.2] \times [0.1, 0.2])$, densely filled by initial points. When $n \rightarrow \infty$, the image of this rectangle gives a dense set along the y -axis. Figure 1(c) shows this image for $n = 80$.

B. Möbius map

Next, we add dissipation to the maps above. This leads to the emergence of regions where the area is contracted and of regions where the area is expanded. This can be accomplished by applying a nontrivial circle map to one of the coordinates (or to both of them). As we want to iterate the resulting map forward and backward, the simplest map $x \rightarrow x + a \sin(x)$ is not practical because it is inconvenient to invert it numerically. Therefore, we use the so-called Möbius map.^{18,19}

The Möbius map (MM) is a circle map $x_n \rightarrow x_{n+1} \pmod{1}$ depending on three parameters $0 \leq u, v < 1$, and $-1 < \varepsilon < 1$,

$$e^{i2\pi(x_{n+1}-v)} = \frac{\varepsilon + e^{i2\pi(x_n-u)}}{\varepsilon e^{i2\pi(x_n-u)} + 1}. \tag{4}$$

For a numerical implementation, it is convenient to rewrite this formula in the real form,

$$\begin{aligned} \cos(2\pi(x_{n+1} - v)) &= \frac{(1 + \varepsilon^2) \cos(2\pi(x_n - u)) + 2\varepsilon}{1 + 2\varepsilon \cos(2\pi(x_n - u)) + \varepsilon^2}, \\ \sin(2\pi(x_{n+1} - v)) &= \frac{(1 - \varepsilon^2) \sin(2\pi(x_n - u))}{1 + 2\varepsilon \cos(2\pi(x_n - u)) + \varepsilon^2}, \end{aligned}$$

and to express x_{n+1} from these equations using the standard ATAN2 function,

$$\begin{aligned} x_{n+1} &= v + \frac{1}{2\pi} \text{ATAN2}((1 - \varepsilon^2) \sin(2\pi(x_n - u)), \\ &\quad \times (1 + \varepsilon^2) \cos(2\pi(x_n - u)) + 2\varepsilon). \end{aligned} \tag{5}$$

Parameter ε determines level of contraction on the circle: for $\varepsilon = 0$, the MM is a circle shift and for $\varepsilon \rightarrow 1$, it maps almost all circle to a small neighborhood of one point on it.

The MM is invertible; its inverse map, as one can easily see from the following representation:

$$M(\varepsilon, u, v) : \tan(\pi(x_{n+1} - v)) = \frac{1 - \varepsilon}{1 + \varepsilon} \tan(\pi(x_n - u)) \tag{6}$$

is also a MM

$$M^{-1}(\varepsilon, u, v) = M(-\varepsilon, v, u). \tag{7}$$

We illustrate the action of MM and its inverse in Fig. 2.

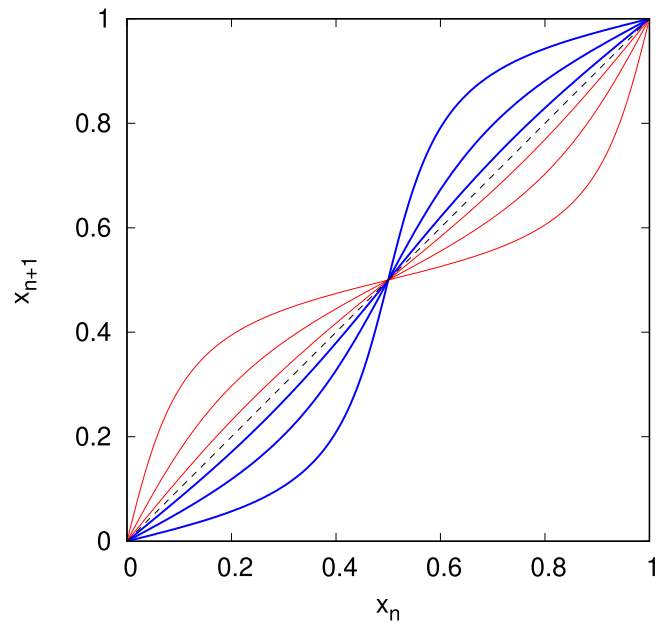


FIG. 2. Möbius map (blue bold lines) $M(\varepsilon, 0, 0)$ and its inverse (red lines) for three values of the contraction parameter $\varepsilon = 0.1, 0.3, 0.6$.

C. Superposition of torus maps with the Möbius map

A combination of the MM with area-preserving torus maps introduced in Sec. II A gives maps on a torus that do not conserve area. We apply the MM with $u = v = 0$ to maps A, C, S in a symmetric way, to preserve symmetry with respect to iterations backward and forward in time,

$$\begin{aligned} A &: \begin{pmatrix} M_\varepsilon & 0 \\ 0 & 1 \end{pmatrix} A \begin{pmatrix} M_\varepsilon & 0 \\ 0 & 1 \end{pmatrix}, & C &: \begin{pmatrix} M_\varepsilon & 0 \\ 0 & 1 \end{pmatrix} C \begin{pmatrix} M_\varepsilon & 0 \\ 0 & 1 \end{pmatrix}, \\ S &: \begin{pmatrix} M_\varepsilon & 0 \\ 0 & 1 \end{pmatrix} S \begin{pmatrix} M_\varepsilon & 0 \\ 0 & 1 \end{pmatrix}. \end{aligned} \tag{8}$$

D. Attractors and repellers in the torus maps

We show attractors and repellers in maps (8) in Fig. 3. Panels (a)–(c) show invariant measures for the attractor and the repeller. We obtain these figures by plotting long trajectories of forward and backward iterations. Panels (d)–(f) aim to illustrate the “backbones” of these sets: in panels (d) and (e), we plot stable (in red) and unstable (in blue) manifolds of the fixed point $(0, 0)$ for maps A and C ; in panel (f), a rational approximation for map S is presented.

For the perturbed Anosov cat map A , both the attractor and the repeller are hyperbolic: all periodic orbits remain saddles, and their stable and unstable manifolds intersect transversally [see Fig. 3(d)]. For small values of the dissipation parameter ε , this follows from the structural stability of hyperbolic chaos under small smooth perturbations. For large ε , hyperbolicity is confirmed numerically. Thus, we can conclude that there exists a pair of SRB

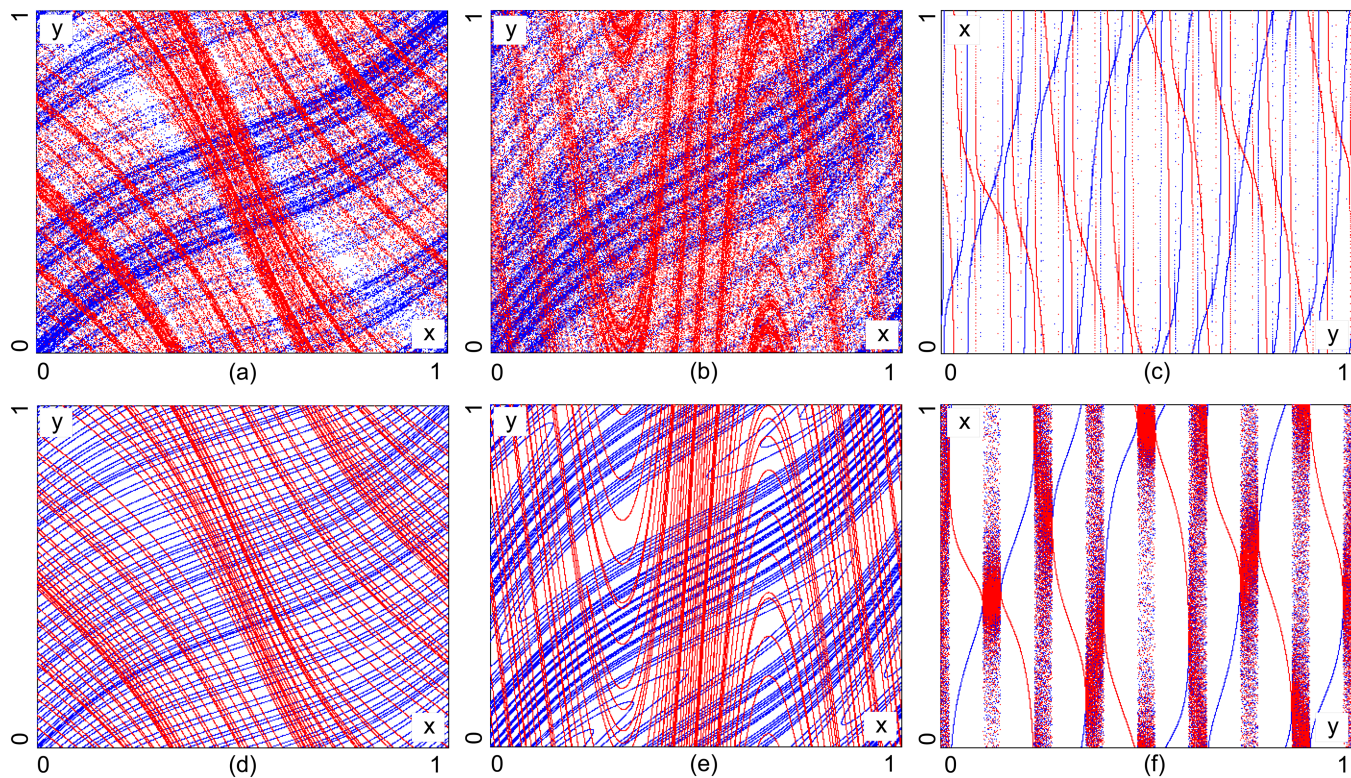


FIG. 3. Forward iterations (blue dots) and backward iterations (red dots) of one of initial conditions for the Anosov cat map [panel (a)], the standard map [panel (b)], and for the Strange nonchaotic attractor (SNA) [panel (c)]. Panels (d) and (e): stable (in red) and unstable (in blue) invariant manifolds of $(0, 0)$ saddle fixed point for the Anosov cat map and the standard map, respectively. Panel (f): the attractor and the repeller for the skew-shift map for a rational $\omega = 5/8$, demonstrating the loss of ergodicity. Parameter of dissipation in the Möbius map in all cases is $\varepsilon = 0.2$.

(Sinai–Ruelle–Bowen)-measures: a forward SRB-measure is associated with the attractor and a backward SRB-measure is associated with the repeller. Figure 3(a) shows the approximation for both forward (in blue color) and backward (in red color) SRB-measures. Figure 3(d) confirms that the forward SRB-measure is concentrated on the unstable invariant manifold, while the backward SRB-measure is concentrated on the stable invariant manifold. Since we break the conservativity, these two measures become mutually singular.¹²

The standard map is not hyperbolic, as tangencies of stable and unstable manifolds of periodic orbits are observed. Correspondingly, small elliptic islands can exist even for large values of parameter K , see Ref. 22. When MM is added, homoclinic tangencies, see Fig. 3(e), generally can give rise to the attracting and repelling orbits instead of elliptic ones.^{24,25} In numerics, we observed them for relatively small values of K . However, for large K , such orbits become “unobservable” [see Fig. 3(b)] because of very narrow basins. The situation here is similar to other nonhyperbolic attractors (the so-called quasiattractors in the sense of Afraimovich and Shilnikov^{26,27}), which can potentially coexist with stable periodic orbits. Correspondingly, nonhyperbolic repellers can coexist with completely unstable periodic orbits (which are stable for backward

iterations). In fact, for large values of K , the perturbed Chirikov map exhibits non-reversible mixed dynamics^{28,29} [see Fig. 3(b)] appearing when a chaotic attractor intersects with a chaotic repeller in a system that is not time-reversible.

It appears that Fig. 3(b) also gives a good approximation for both forward (in blue color) and backward (in red color) measures for the perturbed Chirikov map \mathcal{C} , while Fig. 3(e) shows the unstable (in blue) and stable (in red) invariant manifolds of the zero fixed point in this case. It seems that forward (backward) invariant measure is concentrated here on the unstable (stable) invariant manifold as it was observed in the hyperbolic case [cf. Figs. 3(a) and 3(d) with Figs. 3(b) and 3(e)]. However, there is no theory confirming this fact. Probably, forward (backward) measure is concentrated here on the closure of set of stable (completely unstable) periodic orbits, similar to systems from Newhouse domains.^{8,9,30} However, we cannot see it due to the finiteness of numerics. Thus, we can conclude that from the numerical point of view, the nonhyperbolic Chirikov standard map demonstrates the same chaotic properties as the hyperbolic Anosov cat map.

The third example, the skew-shift map [see Fig. 1(c)], is nonchaotic and belongs to examples of non-chaotic ergodic systems. All unperturbed trajectories here are neutral (have two vanishing

Lyapunov exponents). When dissipation is included via the MM, the exponent in the x -direction becomes negative but the skew-shift structure of the phase space, existing for irrational ω , prevents the appearance of a smooth torus, so the attractor is fractal.³¹ The same holds for the strange non-chaotic repeller. For this example, the structure of the attractor and the repeller can be revealed not through stable and unstable manifolds of a saddle point (which does not exist) but via rational approximations.³² When the parameter ω is rational ($\omega = p/q$), the corresponding map loses ergodicity: the circle shift in variable y on base of which the skew shift is constructed, possesses a continuous set of periodic (with period q) orbits. Correspondingly, the total dynamics can be split in periodically forced combination of a shift in direction x and of the MM. It is known, that superposition of MMs is also a MM. On the other hand, the MM has the following dichotomy: either there is a stable and unstable fixed points, or the dynamics is conjugate to a circle shift, which for generic parameter values is ergodic. Therefore, in dependence on the value of y , the q th iteration of map S with $\omega = p/q$ demonstrates either a point attractor and a point repeller, or an invariant set symmetric with respect to time inverse (altogether there are q sets of each type). These sets are clearly seen in Fig. 3(f). This structure exists for any rational approximation of the irrational parameter ω , and the strange non-chaotic attractor and repeller in Fig. 3(c) can be viewed as “limits” of the corresponding rational approximations, one of which is shown in Fig. 3(f).

E. A chaotic flow on the three-torus

Here, we present an example of overlapping of the attractor and the repeller in the continuous-time dynamics. The minimal dimension of the phase space for such systems is three, and we construct our example on a three-dimensional torus $0 \leq x_i < 1, i = 1, 2, 3$ as follows. First, we take a dynamical system which conserves the phase volume, similar to the three maps described in Sec. II A. We write it as follows:

$$\dot{x}_k = \sum_j (A_{kj} \cos 2\pi x_j + B_{kj} \sin 2\pi x_j + C_{kj} \cos 4\pi x_j + D_{kj} \sin 4\pi x_j). \tag{9}$$

Additionally, we set

$$A_{kk} = B_{kk} = D_{kk} = 0, \quad C_{kk} = \varepsilon,$$

which allows us to control the divergence of the phase volume through parameter ε . For $\varepsilon = 0$, the phase volume is conserved, while for $\varepsilon \neq 0$, it is compressed in one part of the phase space and expands in another part. Our goal is to find an example with chaos in some range of values of ε . Searching sets of the coefficients $A_{kj}, B_{kj}, C_{kj}, D_{kj}$ taken randomly from a uniform distribution on $(-0.5, 0.5)$, we found a set yielding chaotic dynamics in the interval $0 \leq \varepsilon < 0.035$. We checked this by means of the Lyapunov exponents, calculated separately for trajectories of (9) forward and backward in time. The result is presented in Fig. 4. It indicates, that although the system (9) is not expected to be hyperbolic, chaos is persistent at least for small values of the dissipation parameter ε .

While the trajectories of system (9) fill the whole three-dimensional torus in the chaotic regime, it is not easy to represent the dynamics in discrete time, as we have not found a good two-dimensional Poincaré section without tangencies. Thus, we use a

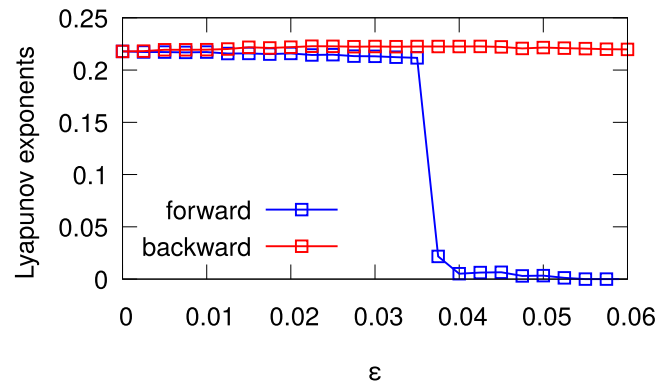


FIG. 4. Lyapunov exponents in system (9) in dependence on the dissipation parameter ε . Blue and red show the largest exponents for forward and backward integration, respectively.

rather arbitrary section $x_3 = 0$ and plot on it points of intersection with a trajectory in both directions, to fill the full square, see Fig. 5. The density of the map is of course non-uniform, it has pronounced minima at the regions around tangencies of the flow (9) with the section plane (i.e., regions where $x_3 = \dot{x}_3 = 0$).

At the end of this section, we would like to mention that equations of type (9) have been recently studied in the context of the phase dynamics of interacting nanomechanical oscillators.³³ In another context, such equations are used to model chaotic stationary Lagrangian trajectories in three-dimensional fluid flows (a prominent example here is the so-called ABC flow³⁴).

III. KANTOROVICH-RUBINSTEIN-WASSERSTEIN DISTANCE BETWEEN THE ATTRACTOR AND THE REPELLER

Kantorovich–Rubinstein–Wasserstein distance (KRWD) is a measure of similarity between two probability measures μ and ν . It is defined as a solution of an optimal transportation problem in the sense of Monge and Kantorovich, namely, as a transportation protocol minimizing the cost needed to transport mass from μ to ν . The most transparent formulation of KRWD is when both measures are weighted sets of point measures (i.e., densities are sets of delta-functions, see Ref. 14),

$$\mu = \sum_{i=1}^{n_1} \alpha_i \delta_{x_i}, \quad \nu = \sum_{j=1}^{n_2} \beta_j \delta_{y_j}.$$

Then, any matrix $f_{ij} \geq 0, 1 \leq i \leq n_1, 1 \leq j \leq n_2$ satisfying

$$\sum_i f_{ij} = \beta_j, \quad \sum_j f_{ij} = \alpha_i$$

delivers a possible transportation that transports one measure into another one. An optimal transportation should minimize the cost function defined according to the “performed work,” i.e., transported mass times the distance $c_{ij} = \|x_i - y_j\|_2$ between two

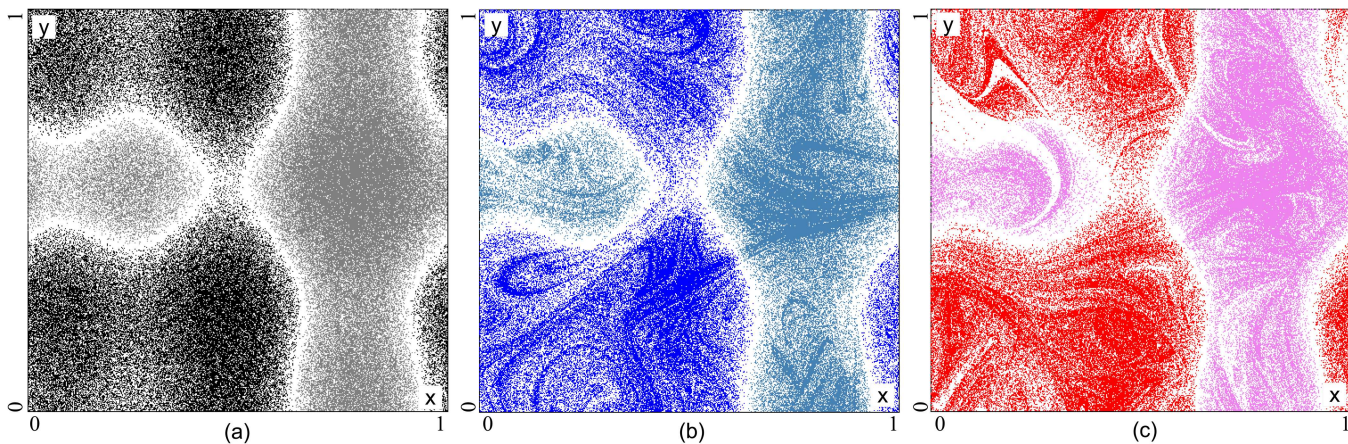


FIG. 5. Poincaré sections of flow (9) at $x_3 = 0$. At each panel, two different colors of points show cross section in one or in another direction (i.e., with $\dot{x}_3 > 0$ and $\dot{x}_3 < 0$). Panel (a): symmetric case $\varepsilon = 0$, the attractor and the repeller coincide. Panel (b): The attractor for $\varepsilon = 0.035$. Panel (c): The repeller for $\varepsilon = 0.035$. Note that the bands with small density (look white) separating regions of two colors correspond to lines of tangencies of the flow with the cross-sectional plane.

points

$$W(\mu, \nu) = \min \sum_{ij} f_{ij} c_{ij}.$$

This minimal cost function is the Kantorovich–Rubinstein–Wasserstein distance $W(\mu, \nu)$. Of course, any metric could be used as “distance” c_{ij} .

In the previous literature, KRWD has been applied to characterize dynamical systems. In Ref. 14, KRWDs between the sets obtained via iterations of a dynamical system (in particular, of the Hénon map) at different parameters have been determined. Furthermore, applicability of KRWD to detect synchronization of two chaotic sets has been discussed. Below, we apply the KRWD to characterize difference between attractors and repellers.

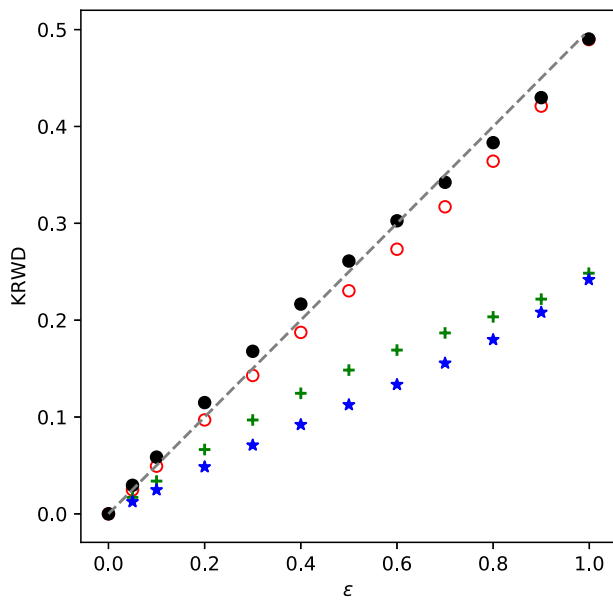
In Fig. 6, we show the results for the Kantorovich–Rubinstein–Wasserstein distance between attractors and repellers for the three maps presented in Sec. II C. The details of calculation are as follows. We first constructed histogram approximations of the probability densities, using a $N \times N$ grid on the unit torus, and 40 000 trajectories (iterated forward and backward, respectively) of length $m = 25\,000$ (totally 10^9 points on both the attractor and the repeller). Then, the Wasserstein distance was calculated according to the definition above, with $n_1 = n_2 = N^2$ (see the Appendix for details). The distance on the torus was defined as $\sqrt{(\Delta x)^2 + (\Delta y)^2}$, where $\Delta x = \min(|x_1 - x_2|, 1 - |x_1 - x_2|)$ and similar for Δy . To check for possible errors due to finite grid, together with the distance according to the constructed $N \times N$ histogram, we used “coarse-grained” distributions on sets $\frac{N}{2} \times \frac{N}{2}$, $\frac{N}{4} \times \frac{N}{4}$, and $\frac{N}{8} \times \frac{N}{8}$. In Fig. 6, we show results for $N = 64$. The distances for $N/2 = 32$ deviated from those at $N = 64$ by less than 0.5%.

One can see from Fig. 6 that in all cases of two-dimensional maps, the distance between the attractor and the repeller, for small value of dissipation parameter ε , grows linearly with ε . Furthermore,

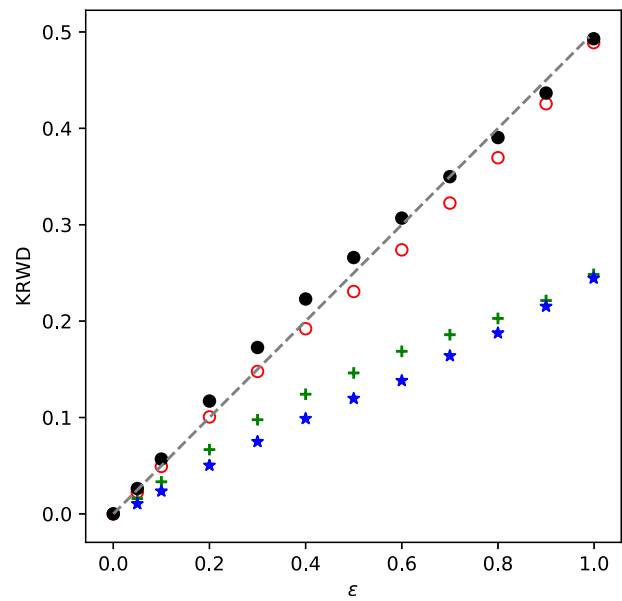
in this figure, we show KRWDs between the attractors and the uniform distribution on the torus and between the repellers and the uniform distribution and also observe a linear growth. Curiously, in Figs. 6(a) and 6(b), the sum of distances to the uniform distribution is almost equal to the attractor–repeller distance; in Fig. 6(c), these values differ significantly. However, the deviation is not very large, which allows one to speak about certain “symmetry” of the attractor and repeller measures with respect to the uniform one.

It is interesting to consider the limit $\varepsilon \rightarrow 1$. For the one-dimensional Möbius map, at ε close to 1, the point 0 is a strong attractor, and the point 0.5 is a strong repeller (see Fig. 2). Due to this, in the two-dimensional maps under consideration, it is natural to expect that for $\varepsilon \rightarrow 1$ attractors are close to the line $x = 0$, $0 \leq y < 1$ and repellers are close to the line $x = 0.5$, $0 \leq y < 1$. Indeed, this is confirmed by Fig. 7, where the attractors and repellers at $\varepsilon = 0.99$ for all above maps are presented. KRWDs in this case is just the area between these two “lines,” which is equal to 0.5 (half period of the MM). This asymptotic value is in good agreement with numerical results presented in Fig. 3 at large values of ε .

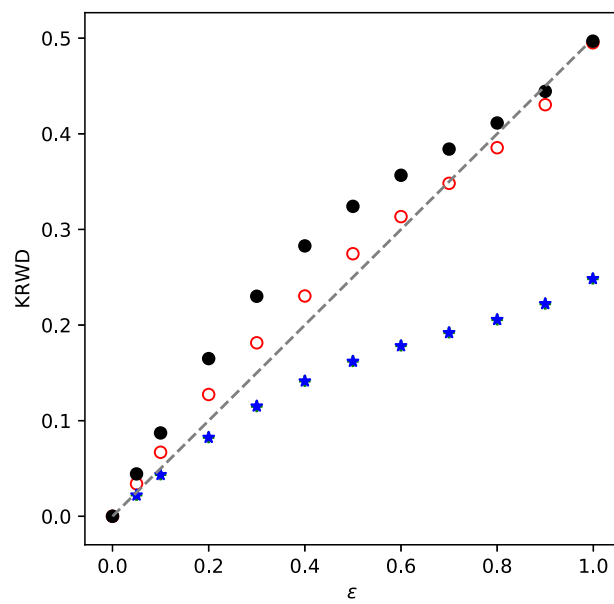
Finally, we present the results for the calculation of the KRWD between the attractor and the repeller for the continuous-time flow (9) (see Fig. 8). Figure 8(a) shows the distance between the attractor and the repeller for the chaotic flow (9) on a three-dimensional torus, while Fig. 8(b) shows the distance for the corresponding two-dimensional Poincaré map. For constructing probability histograms on three-dimensional torus, we use partition of three-torus into $16 \times 16 \times 16$ cells and for the two-dimensional Poincaré map, we apply the same partition as for other two-dimensional maps. We note that these results are very much similar to those for the two-dimensional maps with nearly linear growth of the distance as a function of the dissipation parameter. It is curious that KRWD calculated for initial flow (9) is almost the same as KRWD calculated for its two-dimensional Poincaré map.



a)



b)



c)

FIG. 6. Results of calculation of the KRWD for the Anosov cat map [panel (a)], the standard map [panel (b)], and for the SNA [panel (c)]. Red circles: distances between the attractor and the repeller; green pluses: distances between the attractor and uniform distribution; and blue stars: distances between repellers and uniform distribution [on panel (c) stars overlap with pluses]. Black filled circles: sums of values presented with pluses and stars. Dashed straight lines have a slope of 0.5.

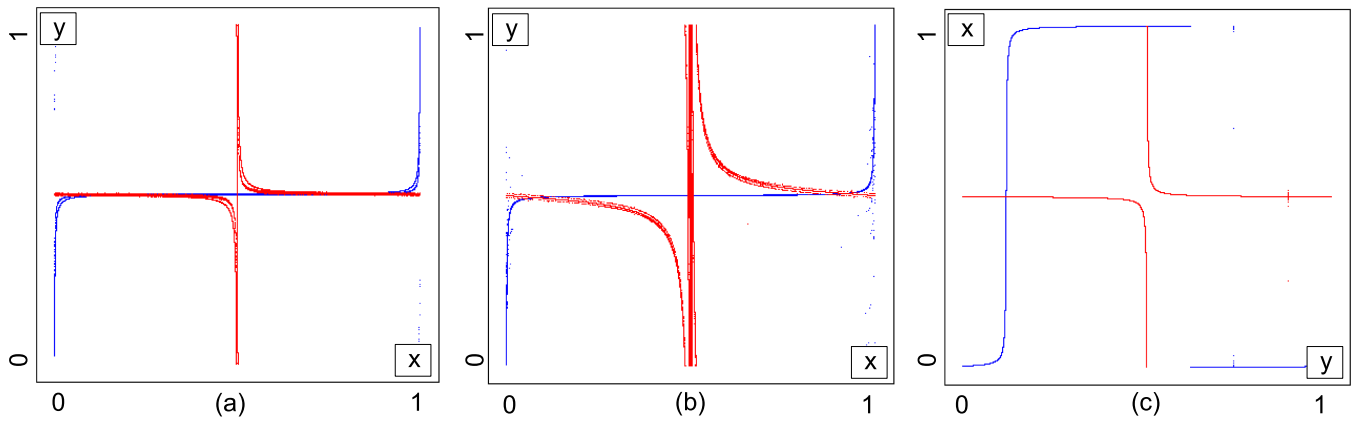


FIG. 7. Phase portraits of the attractor (blue points) and the repeller (red points) for the perturbed Anosov can map [panel (a)], the Chirikov standard map [panel (b)], and the skew-shift map [panel (c)]. In all cases, parameter of dissipation in the Möbius map is $\varepsilon = 0.99$.

IV. DISCUSSION

In summary, we have provided four simple examples of overlapping attractors and repellers on a two-dimensional torus and have characterized the difference between them with the Kantorovich–Rubinstein–Wasserstein distance. In all cases, we have found that the distance grows, at small perturbations of the ideal case where the attractor and the repeller coincide, linearly with the dissipation parameter, which is introduced to break the time-reversal symmetry, for small values of this parameter. For

two-dimensional maps, we have considered only the cases when a Möbius map was applied only to one coordinate on the torus, where its effect on the dynamics is not dramatic (and, in particular, the support of both the attractor and the repeller remains the full torus). In some situations, e.g., when MM with sufficiently large dissipation parameter ε is applied to both coordinates on a torus, we expect that under strong dissipation the topological properties of these sets may change, for example, in the Anosov map, a DA-attractor¹ could appear; this issue is under investigation. Another

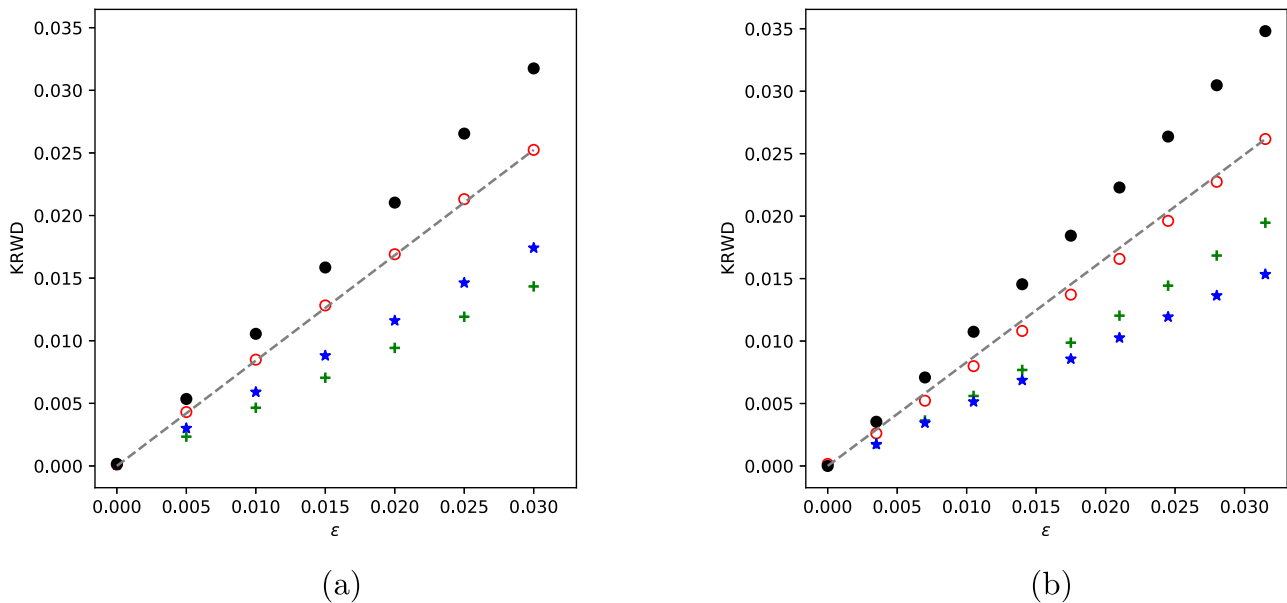


FIG. 8. Distances between the attractor and the repeller for the chaotic flow (9) on a three-dimensional torus [panel (a), partition $16 \times 16 \times 16$] and on Poincaré section [panel (b), partition 64×64]. As in Fig. 6, the markers in panel (a) show distances of the attractor–repeller (red circles), attractor-invariant conservative (green pluses), and repeller-invariant conservative (blue crosses); black circles are sums of green and blue values. In panel (b), green pluses and blue stars are distances not to the uniform distribution but to the invariant distribution at $\varepsilon = 0$ [see Fig. 5(a)]. Dashed gray straight lines are drawn to illustrate nearly linear dependence of KRWD on ε .

interesting phenomenon is connected with a possibility of the de-splitting of the attractor and the repeller according to a bifurcation described in Refs. 4, 5, and 11.

Both the attractor and the repeller in considered examples are fractal sets, but the fractal properties can be hardly deduced from the KRWD, which equally works for smooth and fractal measures. There are approaches for determining mutual singularities of two fractal measures,^{35–37} and their applications to the characterization of attractors and repellers studied above will be presented elsewhere.

Finally, we note that we have characterized overlapping attractors and repellers using KRWD only for simple basic examples. It is known that such an overlapping can also appear in more complex maps including reversible and nonreversible maps arising as a Poincaré section for various problems from application. In particular, such a phenomenon has been observed in the models of coupled oscillators,^{7,10,28,38} in nonholonomic models,^{39–41} in models of vortex dynamics,^{11,42} etc. The study of attractor–repeller merger in these problems using the presented approach appears promising. We expect that the proposed methods can help us to characterize quantitatively the mixed dynamics phenomenon in such problems.

ACKNOWLEDGMENTS

We thank S. Gonchenko, D. Turaev, G. Mantica, and D. Malyshv for fruitful discussions. This paper was supported by the RSF (Grant No. 17-11-01041). Numerical experiments in Sec. III were supported by the Laboratory of Dynamical Systems and Applications NRU HSE of the Russian Ministry of Science and Higher Education (Grant No. 075-15-2019-1931). A. Kazakov also acknowledges financial support of the Ministry of Science and Higher Education of Russian Federation (Project No. 0729-2020-0036).

APPENDIX: SOME DETAILS ABOUT KRWD CALCULATION

Here, we give a short discussion on the numerical implementation of the KRWD calculations. We used two freely available codes,^{43,44} both based on the primal simplex method, which yielded,

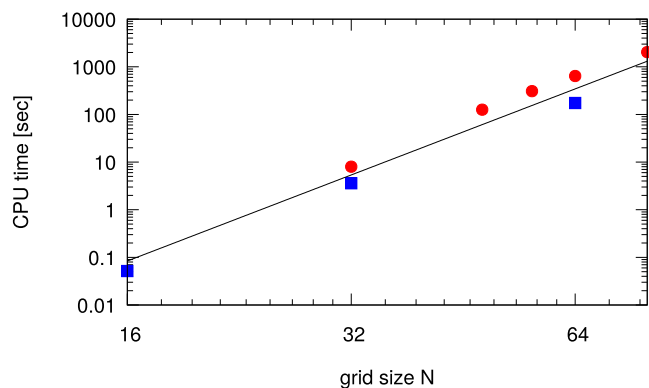


FIG. 9. CPU times vs grid size N for calculation of the KRWD with code⁴³ (based on the algorithm described by Jensen,⁴⁵ red circles) and with code⁴⁴ (based on the primal method for solving a simplex problem, blue squares). The line shows the power law $\sim N^6$.

of course, coinciding results. Although, in general, a solution of the transportation problem may be non-polynomial, in our examples, we observed in all cases a polynomial dependence of the CPU time on the partition size. We illustrate this in Fig. 9. This graph shows the power law $\sim N^6$.

DATA AVAILABILITY

All numerical experiments with two-dimensional maps are described in the paper and can be reproduced without additional information. Parameter values for the solutions of the continuous-time model (9) are available from the corresponding author upon reasonable request.

REFERENCES

- C. Robinson, *Dynamical Systems: Stability, Symbolic Dynamics, and Chaos* (CRC Press, Boca Raton, 1999).
- R. L. Devaney, "Reversible diffeomorphisms and flows," *Trans. Am. Math. Soc.* **218**, 89–113 (1976).
- M. B. Sevryuk, *Reversible Systems* (Springer, 2006), Vol. 1211.
- C. Grebogi, E. Ott, and J. A. Yorke, "Fractal basin boundaries, long-lived chaotic transients, and unstable-unstable pair bifurcation," *Phys. Rev. Lett.* **50**, 935–938 (1983).
- A. Pikovsky, G. Osipov, M. Rosenblum, M. Zaks, and J. Kurths, "Attractor-repeller collision and eyelet intermittency at the transition to phase synchronization," *Phys. Rev. Lett.* **79**, 47–50 (1997).
- A. O. Kazakov, "On the appearance of mixed dynamics as a result of collision of strange attractors and repellers in reversible systems," *Radiophys. Quantum Electron.* **61**, 650–658 (2019).
- D. Topaj and A. Pikovsky, "Reversibility vs synchronization in oscillator lattices," *Physica D* **170**, 118–130 (2002).
- S. V. Gonchenko, L. P. Shilnikov, and D. V. Turaev, "On Newhouse domains of two-dimensional diffeomorphisms which are close to a diffeomorphism with a structurally unstable heteroclinic cycle," in *Proceedings of the Steklov Institute of Mathematics* (Springer, 1997), Vol. 216, pp. 70–118.
- S. V. Gonchenko and D. V. Turaev, "On three types of dynamics and the notion of attractor," *Proc. Steklov Inst. Math.* **297**, 116–137 (2017).
- A. S. Gonchenko, S. V. Gonchenko, A. O. Kazakov, and D. V. Turaev, "On the phenomenon of mixed dynamics in Pikovsky–Topaj system of coupled rotators," *Physica D* **350**, 45–57 (2017).
- A. Kazakov, "Merger of a Hénon-like attractor with a Hénon-like repeller in a model of vortex dynamics," *Chaos* **30**, 011105 (2020).
- G. Gallavotti and E. G. D. Cohen, "Dynamical ensembles in stationary states," *J. Stat. Phys.* **80**, 931–970 (1995).
- W. G. Hoover, O. Kum, and H. A. Posch, "Time-reversible dissipative ergodic maps," *Phys. Rev. E* **53**, 2123 (1996).
- M. Muskulus and S. Verduyn-Lunel, "Wasserstein distances in the analysis of time series and dynamical systems," *Physica D* **240**, 45–58 (2011).
- J. M. Fraser, "First and second moments for self-similar couplings and Wasserstein distances," *Math. Nachr.* **288**, 2028–2041 (2015).
- I. Cipriano and M. Pollicott, "Stationary measures associated to analytic iterated function schemes," *Math. Nachr.* **291**, 1049–1054 (2018).
- C. Villani, *Optimal Transport. Old and New* (Springer, Berlin, 2009).
- S. A. Marvel, R. E. Mirollo, and S. H. Strogatz, "Phase oscillators with global sinusoidal coupling evolve by Möbius group action," *Chaos* **19**, 043104 (2009).
- C. C. Gong, R. Toenjes, and A. Pikovsky, "Coupled Möbius maps as a tool to model Kuramoto phase synchronization," arXiv: 2001.07593 (2020).
- A. Katok and B. Hasselblatt, *Introduction to the Modern Theory of Dynamical Systems* (Cambridge University Press, 1995).
- B. Chirikov and D. Shepelyansky, "Chirikov standard map," *Scholarpedia* **3**, 3550 (2008).
- P. Duarte, "Plenty of elliptic islands for the standard family of area preserving maps," in *Annales de l'Institut Henri Poincaré (C) Non Linear Analysis* (Elsevier, 1994), Vol. 11, pp. 359–409.

- ²³I. P. Cornfeld, S. V. Fomin, and Ya. G. Sinai, *Ergodic Theory* (Springer, New York, 1982).
- ²⁴N. K. Gavrilov and L. P. Shilnikov, "On three-dimensional dynamical systems close to systems with a structurally unstable homoclinic curve. I," *Math. USSR Sbornik* **17**, 467 (1972).
- ²⁵N. K. Gavrilov and L. P. Shilnikov, "On three-dimensional dynamical systems close to systems with a structurally unstable homoclinic curve. II," *Math. USSR Sbornik* **19**, 139 (1973).
- ²⁶V. S. Afraimovich and L. P. Shilnikov, *Strange Attractors and Quasiattractors in Nonlinear Dynamics and Turbulence*, edited by G. I. Barenblatt, G. Iooss, and D. D. Joseph (Pitman, New York, 1983).
- ²⁷S. V. Gonchenko, L. P. Shilnikov, and D. V. Turaev, "Quasiattractors and homoclinic tangencies," *Comput. Math. Appl.* **34**, 195–227 (1997).
- ²⁸A. A. Emelianova and V. I. Nekorkin, "On the intersection of a chaotic attractor and a chaotic repeller in the system of two adaptively coupled phase oscillators," *Chaos* **29**, 111102 (2019).
- ²⁹A. A. Emelianova and V. I. Nekorkin, "The third type of chaos in a system of two adaptively coupled phase oscillators," *Chaos* **30**, 051105 (2020).
- ³⁰S. E. Newhouse, "The abundance of wild hyperbolic sets and non-smooth stable sets for diffeomorphisms," *Publ. Math. IHÉS* **50**, 101–151 (1979).
- ³¹B. R. Hunt and E. Ott, "Fractal properties of robust strange nonchaotic attractors," *Phys. Rev. Lett.* **87**, 254101 (2001).
- ³²U. Feudel, S. P. Kuznetsov, and A. Pikovsky, *Strange Nonchaotic Attractors. Dynamics between Order and Chaos in Quasiperiodically Forced Systems* (World Scientific, Singapore, 2006).
- ³³M. H. Matheny, J. Emenheiser, W. Fon, A. Chapman, A. Salova, M. Rohden, J. Li, M. Hudoba de Bady, M. P'osfai, L. Duenas-Osorio, M. Mesbahi, J. P. Crutchfield, M. C. Cross, R. M. D'Souza, and M. L. Roukes, "Exotic states in a simple network of nanoelectromechanical oscillators," *Science* **363**, eaav7932 (2019).
- ³⁴T. Dombre, U. Frisch, J. M. Greene, M. Hénon, A. Mehr, and A. M. Soward, "Chaotic streamlines in the ABC flows," *J. Fluid Mech.* **167**, 353 (1986).
- ³⁵H. Kantz, "Quantifying the closeness of fractal measures," *Phys. Rev. E* **49**, 5091–5097 (1994).
- ³⁶R. H. Riedi and I. Scheuring, "Conditional and relative multifractal spectra," *Fractals* **5**, 153–168 (1997).
- ³⁷W. J. Xie, Z. Q. Jiang, G. F. Gu, X. Xiong, and W. X. Zhou, "Joint multifractal analysis based on the partition function approach: Analytical analysis, numerical simulation and empirical application," *New J. Phys.* **17**, 103020 (2015).
- ³⁸O. Burylko, A. Mielke, M. Wolfrum, and S. Yanchuk, "Coexistence of Hamiltonian-like and dissipative dynamics in rings of coupled phase oscillators with skew-symmetric coupling," *SIAM J. Appl. Dyn. Syst.* **17**, 2076–2105 (2018).
- ³⁹A. V. Borisov, I. S. Mamaev, and I. A. Bizyaev, "The hierarchy of dynamics of a rigid body rolling without slipping and spinning on a plane and a sphere," *Regul. Chaotic Dyn.* **18**, 277–328 (2013).
- ⁴⁰A. S. Gonchenko, S. V. Gonchenko, and A. O. Kazakov, "Richness of chaotic dynamics in nonholonomic models of a celtic stone," *Regul. Chaotic Dyn.* **18**, 521–538 (2013).
- ⁴¹I. A. Bizyaev, A. V. Borisov, and A. O. Kazakov, "Dynamics of the Suslov problem in a gravitational field: Reversal and strange attractors," *Regul. Chaotic Dyn.* **20**, 605–626 (2015).
- ⁴²E. V. Vetchanin and I. S. Mamaev, "Dynamics of two point vortices in an external compressible shear flow," *Regul. Chaotic Dyn.* **22**, 893–908 (2017).
- ⁴³G. Doran, "PyEMD: Earth mover's distance for Python" (2014), see <https://github.com/garydoranjr/pyemd> (accessed May 2020).
- ⁴⁴J. Forrest, D. de la Nuez, and R. Lougee-Heimer, "CLP: COIN linear program code" (2004), see <https://www.coin-or.org/Clp/index.html> (accessed May 2020).
- ⁴⁵P. Jensen, "Operation research methods" (1999), see <https://www.me.utexas.edu/jensen/methods/net.pdf/nettrans.pdf> (accessed May 2020).